J. Geogr. Sci. 2019, 29(2): 306-320
DOI: https://doi.org/10.1007/s11442-019-1598-x

Evolution of the gravel-bedded anastomosing river within the Qihama reach of the First Great Bend of the Yellow River

GAO Chao[1,2], WANG Suiji[1,2]

1. Key Laboratory of Water Cycle and Related Land Surface Processes, Institute of Geographic Sciences and Natural Resources Research, CAS, Beijing 100101, China;
2. College of Resources and Environment, University of Chinese Academy of Sciences, Beijing 100049, China

Abstract: The anastomosing river that is present within the First Great Bend of the Yellow River is different from other sand-bedded rivers of this type because it contains gravel-bedded materials. It is therefore important to determine whether, or not, the specific characteristics of this anastomosing river are similar to those seen in sand-bedded forms, including the characteristics of erosion and deposition, and the stability of channel and interchannel wetlands. Four Landsat images from 1990, 2001, 2013, and 2016 alongside two Google Earth (GE) images from 2011 and 2013 were utilized in this study in tandem with field sampling and observations to select a 12 km main channel length section of the Qihama reach anastomosing river. This section was then used to determine variations in channel planform and sedimentary characteristics over a 26 year period. The results of this study show that this gravel-bedded anastomosing river has exhibited a high degree of stability overall, and that there has been no obvious channel and wetland bank erosion and deposition. Data also show that over the 26 years of this study, anastomosing belt area increased by 2.43%, while the ratio of land to water area remained almost equal. The number of wetlands has also increased along this river section at a rate as high as 62.16% because of the fragmentation of some small interchannel examples, while the talweg has alternately migrated to either the left or right over long periods of time at a relatively stable rate. Indeed, as a result of the migration of this line, there has been significant turnover in the number of islands within the main channel while bank shift has occurred at a rate of about 5 m/yr. The numerous anastomosing channels within this river section remained very stable over the course of this study, characterized by a mean annual migration rate of just 1 m/yr, while the sediments in bank columnar sections are mainly composed of fine sands or silts with a relatively high clay content. The sediment grain-size distribution curve for this river section contains multiple peaks, distinct from the muddy sediments within bank columnar sections from sand-bedded anastomosing rivers. The dense vegetation within riparian and interchannel wetlands alongside this river reach has also protected anastomosing channels from erosion and maintained

Received: 2017-12-15 **Accepted:** 2018-03-09
Foundation: National Natural Science Foundation of China, No.41571005, No.41271027
Author: Gao Chao, Master Candidate, specialized in fluvial geomorphology. E-mail: gaoc.15s@igsnrr.ac.cn
*Corresponding author: Wang Suiji, PhD and Associate Professor, specialized in fluvial geomorphology and fluvial sedimentology. E-mail: wangsj@igsnrr.ac.cn

their stability, a key feature of this gravel-bedded system.

Keywords: gravel-bedded anastomosing river; anastomosing belt; wetlands; talweg; sediments; Yellow River

1 Introduction

Anastomosing rivers are stable and interconnected multi-channel systems that differ from other waterway patterns and have attracted an increasing amount of research attention over recent decades. In his early work, Schumm (1968) was the first to differentiate anastomosing rivers from their braided counterparts, noting that the former are stable and comprised of low gradient multichannel systems that form on alluvial plains because of low water transport capacity which leads to riverbed deposition and branching. Although Rust (1978) later differentiated anastomosing rivers from other forms using the braided index and their degree of sinuosity, later workers have noted severe limitations in the use of these semi-quantitative indexes (Wang *et al*., 2002). Smith and Smith (1980) subsequently published a more detailed analysis of this type of watercourse, noting that an anatomosing river comprises a stable multichannel system with a low gradient, a medium amount of bending, and a series of interconnected channels separated by wetlands that themselves contain vegetation. Building on this early study, a detailed series of studies on anastomosing rivers have resulted from subsequent research (e.g., Schumm, 1985; Selby, 1985; Knighton and Nanson, 1993; Wang and Ren, 1999; Wang *et al*., 1999, 2004, 2005; Wang and Yin, 2000; Makaske, 2001; Wang, 2002) leading to classifications that are mainly based on traditional geomorphological methods. Thus, although anatomosing rivers have traditionally been classified based on the degree of sediment transport, sedimentation rate, and the presence and shape of channel planforms, technological developments and the emergence of computational mathematics has enabled simulation-based research on river networks. In this context, Wang (1990) first introduced the concept and method of applying fuzzy mathematics to problems in river classification, presenting analyses of some examples, while Shi *et al*. (2007a) classified the different watercourse types present within the lower reaches of the Yellow River by applying fuzzy clustering and discriminate analyses. Indeed, by making a number of improvements to the application of fuzzy clustering, these workers were able to conclude that some discriminants and criteria used in river classification established via these statistical methods were invalid (Shi *et al*., 2007b, 2009; Xu and Shi, 2009). At the same time, other researchers have also applied the cellular automata method to simulate the processes of braided river formation (e.g., Murray and Paola, 1994, 2015; Thomas and Nicholas, 2002). These methods, however, rely excessively on computer analyses while the index they utilize to generate models is relatively simple because the interactions between various factors are ignored. Some studies in this area have also been focused solely on the pattern of single rivers, so cannot be more widely applied in fluvial geomorphology.

A number of typical anastomosing rivers are known globally, including the lower reaches of the Saskatchewan River, the upper reaches of the Columbia River, the Wakool River in Canada, Cooper's Creek in Australia, and the Rhine-Meuse Delta in the Netherlands (Smith and Putnam, 1980; Rust, 1981; Smith, 1983; Tornqvist, 1993). Rivers of this type within China are most obvious in the section between Songzikou and other estuaries that divert the Yangtze River and Dongting Lake, the reach adjacent to the confluence of the Heilong and the Songhua rivers, and in the waterway section within the Pearl River Delta (Wang *et al*.,

1999). Although these waterways have commonly been referred to as "sandy anastomosing rivers" because of the presence of sediments of this size within their channel beds, Wang (2008) identified a new sub-type when studying river transformation patterns within the Yellow River Basin. This new sub-type does not differ from more common sandy anastomosing rivers in planform, micro-geomorphology, and other features other than in the presence of a gravel bed; these rivers are therefore considered to belong to a new subclass of anastomosing river, distinct and worthy of study in terms of scouring and silting characteristics, the causes underlying their formation, and the maintenance of channel and interchannel wetlands. All of these aspects are interesting in the context of current fluvial geomorphological and river sedimentological research.

The First Great Bend within the Maqu reach of the Yellow River formed as a result of uplift of the Qinghai-Tibet Plateau and has been less influenced by human activities because of its unique geographical location and environmental characteristics. This region is therefore ideal to study the evolution of rivers under natural conditions. Indeed, previous research that has evaluated the fluvial geomorphology of the Yellow River on the Qinghai-Tibet Plateau has mainly been focused on its formation, development, and evolution over geological time scales (e.g., Yuan and Wang, 1995; Li *et al*., 1996; Yang and Wang, 1996; Zhang *et al*., 2003), and more recent processes and characteristics have rarely been investigated (Wang, 2008; Li *et al*., 2013). Recently, however, Liu and Wang (2017) discussed variations in interchannel wetlands within the Maqu anastomosing river reach of the Upper Yellow River. The results of this study revealed the spatial distribution and level of interchannel wetland development within this gravel-bedded anastomosing river for the first time. Four Landsat images (1990, 2001, 2013, and 2016) and two Google Earth (GE) images (2011 and 2013) of a 12-km main channel length section of the Qihama anastomosing river reach are used in this study, in combination with field observations and sampling, to analyze variations in channel planform and sedimentary characteristics over a 26-year period. The objective of this study is to explore the evolutionary characteristics of a gravel-bedded anastomosing river under natural conditions in order to enhance our understanding of this new river sub-pattern, and enrich the theoretical basis of fluvial geomorphology.

2 Study area and methods

2.1 Study area

The study area discussed in this paper has an elevation of about 3400 m and is located in the vicinity of Qihama Town (33°N, 102°E) at the start of the First Great Bend of the Yellow River (Figure 1), in the southwestern Gannan Grassland. The mean annual precipitation in this region is 520 mm, mean annual temperature is 2°C, and the frost-free period is 120 days. The main channel selected for analysis is about 12 km in length, has a mean gradient about 0.60‰ (Li *et al*., 2013), and a mean channel width of about 200 m. The main channel and anabranches with varying degrees of sinuosity and width are connected to one another along this section; ratios of their width to depth are all below 40 and sometimes about 20. Dense trees, shrubs, and grasses grow on interchannel wetlands around this river section, have a surface sediment thickness between 1 m and 2.3 m, and are mainly comprised of mud and silt. The sediment that makes up the river bed is mostly gravel that has a median grain size

between 4 cm and 7 cm (Wang, 2008). Hydrological data recorded at the Maqu gauging station adjacent to the study area shows that mean annual runoff is 14.4 billion m^3; runoff between June and October accounts for about 73% of the annual volume, and peak flow normally reaches a maximum in July and September when mean monthly values are 1046.74 m^3/s and 955.19 m^3/s, respectively. Data also show that the mean annual suspended sediment load is 4.47 million tons, and the period between May and October accounts for about 95% of the annual total.

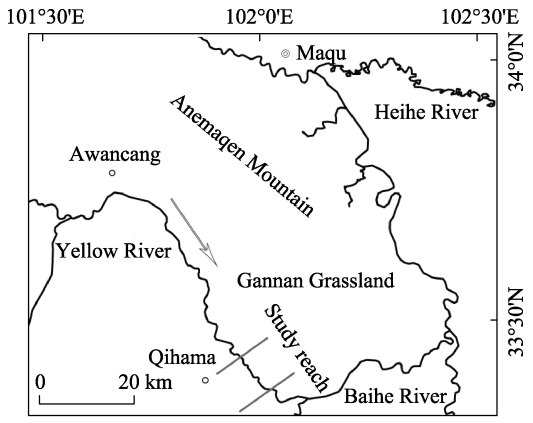

Figure 1 Map showing the location of the river reach discussed in this study

2.2 Methods

Satellite image analysis is an important and powerful tool used to obtain channel planforms that has been widely applied in fluvial geomorphological research (e.g., Wang *et al*., 2014; Mei and Wang, 2016). The Landsat images of the study area used in this research comprise 30 m resolution TM data (captured on July 8th, 1990), 15 m resolution ETM data (captured on August 15th, 2001), and 15 m resolution OLI data (captured on July 23rd, 2013, and July 15th, 2016). All of these satellite images were downloaded from the United States Geological Survey (http://glovis.usgs.gov/) and were used in combination with two GE images (captured on August 27th, 2011, and July 29th, 2013) that have 0.5 m resolution. All images were collected during the flooding season between June and September in order to facilitate the use of vegetation boundaries to delineate channels and to accurately extract their spatial distributions (Wang *et al*., 2014; Gurnell, 2015; Mei and Wang, 2016).

Image geometric correction was performed using the software ENVI5.1, and the 30 m resolution TM data was resampled using cubic convolution to enhance its resolution to 15 m. All images were then loaded into the software Arcgis10.2 for vectorization and to enable a channel planform to be generated for each year (Figure 2).The TM and ETM data were then processed using standard false color synthesis of bands 4, 3, and 2 while the OLI data were processed using bands 5, 4, and 3 to highlight channel boundaries. A talweg is the line of maximum velocity within each channel section and also delineates the deep connection that forms during interactions between water flow and the river bed. These lines are therefore drawn according to the principle that the deeper the water, the higher grayscale value an image will exhibit (Yan *et al*., 2013).The geometric parameters of channel planforms between 1990 and 2016 were therefore calculated quantitatively using the software Arcgis10.2 (Table 1).

A 12 day field survey was also carried out between April 24th, 2016, and May 5th, 2016, and a number of bank columnar sections were sampled. These samples were analyzed at the Institute of Geographic Sciences and Natural Resources Research, CAS, using a Mastersizer 2000 laser particle size analyzer with a measurement range between 0.01 μm and 2000 μm and an error less than 2%. Particle size (d_m) was transformed into φ value using the formula proposed by Udden (1914) and Wentworth (1922), as follows:

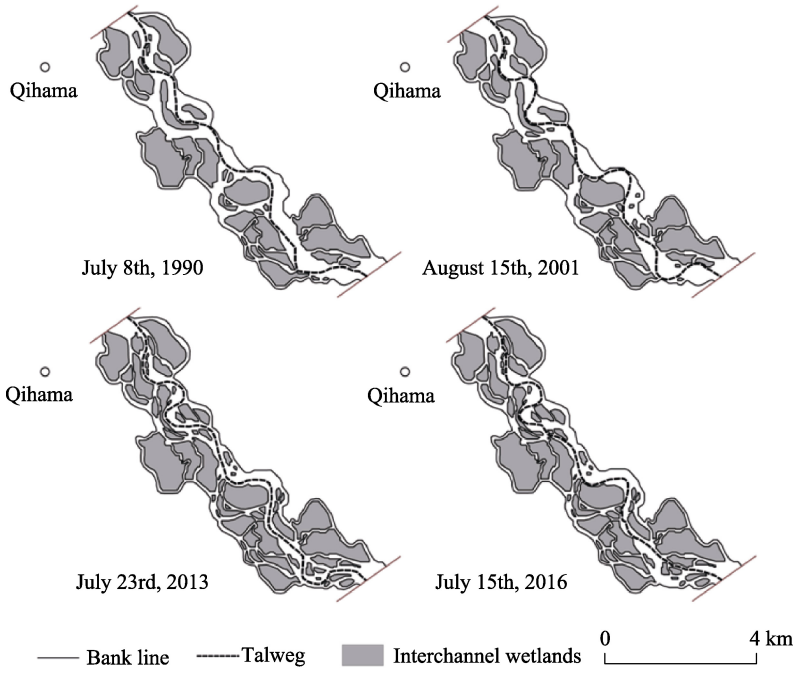

Figure 2 Channel planforms in different years within the river reach studied in this paper

$$\varphi = -\log_2 d_m \tag{1}$$

Results were then scaled so that values between 1 φ and 2 φ denote coarse sand, while values between 2 φ and 3 φ denote fine sand, values between 3 φ and 4 φ denote very fine sand, values between 4 φ and 8 φ denote silt, values greater than 8 φ denote clay, and values greater than 8 φ denote muddy sediment.

Table 1 Geometric parameters of channel planforms in different years

Date of image captured	Talweg length (km)	Sinuosity	Area of the anastomosing belt (km^2)	Land area (km^2)	Water area (km^2)	Number of wetlands
July 8th, 1990	11.43	1.21	16.89	8.12	8.77	37
August 15th, 2001	12.83	1.36	17.00	8.27	8.73	40
July 23rd, 2013	12.72	1.35	17.17	9.12	8.05	60
July 15th, 2016	12.18	1.29	17.30	9.11	8.19	60

3 Results

3.1 Variation in channel planform parameters

The data presented in Figure 3a show that the ratio between water and land areas within the anastomosing belt of this river reach remained almost equal over the course of this study and did not change significantly. Results show, for example, that water and land area percentages were 52% and 48% in 1990, 51% and 49% in 2001, 53% and 47% in 2013, and 53% and 47% in 2016, respectively. This means that the area of the anastomosing belt (i.e., water area plus land area) increased slightly between 1990 and 2016 from 16.89 km^2 to 17.30 km^2, a rate of just 2.43% (Figure 3b), while the length of the talweg increased between 1990 and

2001 and then decreased; the maximum and minimum recorded values were 12.83 km in 2001 and 11.43 km in 1990, respectively. The length of the talweg followed the same increasing trend as the anastomosing belt area between 1990 and 2001, while the opposite trend was seen between 2001 and 2016.

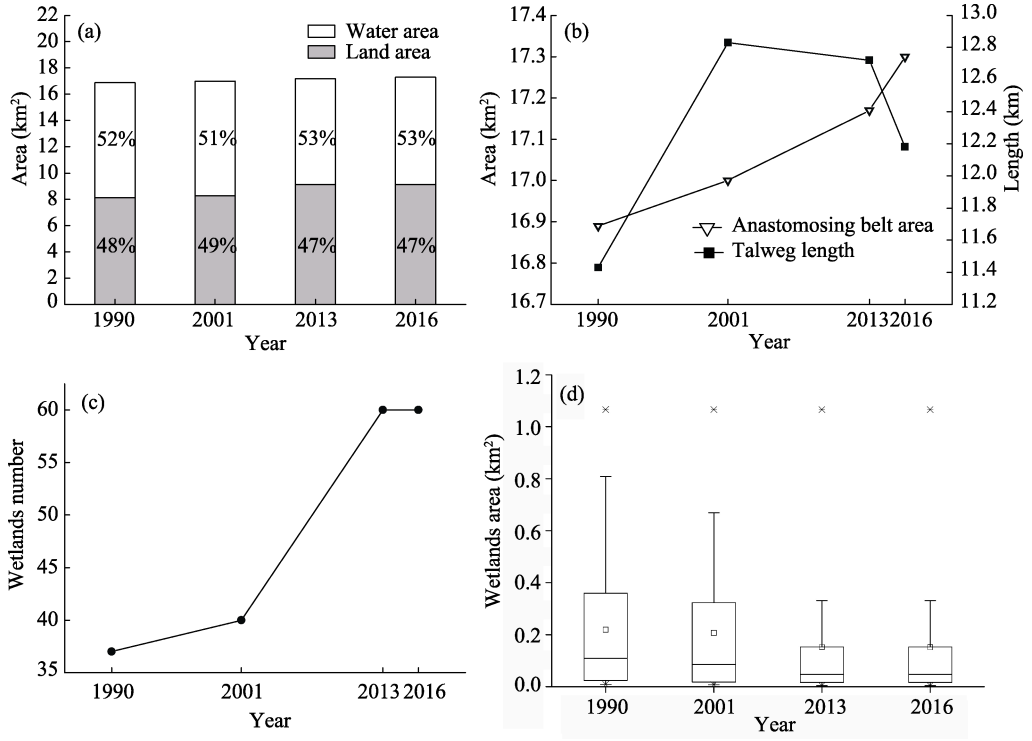

Figure 3 The relative proportions of water and land area (a), variations in anastomosing belt area and talweg length (b), variations in the number of interchannel wetlands (c), and the area of interchannel wetlands within the river reach studied in this paper (d)

The results of this study show that 37, 40, 60, and 60 interchannel wetlands were present within the river reach in 1990, 2001, 2013, and 2016, respectively (Figure 3c). These correspond to the number and rate increases of 3 and 8.11% between 1990 and 2001, and 20 and 50% between 2001 and 2013, respectively. Data show that while the number of interchannel wetlands greatly increased between 2001 and 2013 (Figure 3c), the corresponding increase in area was very small (Figure 3a); this suggests that the interchannel wetlands within the river reach were partially fragmented, a phenomenon that is also reflected by the data presented in Figure 3d. These data (Figure 3d) show that mean areas of interchannel wetlands were 0.22 km^2, 0.21 km^2, 0.15 km^2, and 0.15 km^2 in 1990, 2001, 2013, and 2016, while median areas were 0.11 km^2, 0.09 km^2, 0.05 km^2, and 0.05 km^2, respectively, all significantly decreasing trend. In addition, abnormal values (maximum and minimum) and lower quartiles for these years remained almost unchanged, while the upper edges and quartiles in this box-plot gradually reduced so that the latter was equal to the mean value in 2013 and 2016 (i.e., 75% of wetland area is at the mean level). All these data show that interchannel wetlands within the river reach fragmented overtime; this change is particularly evident for interchannel wetlands with areas between 0.1 km^2 and 0.8 km^2, while not obvious for those

with areas less than 0.1 km^2 or greater than 0.8 km^2. This increase in the number of inter-channel wetlands indicates that some new small channels were formed via flood avulsion on original surfaces, a result that is consistent with the developmental model for sandy anastomosing channels on floodplains (Wang, 2002; Wang *et al*., 2005).

3.2 Talweg migration rate and anastomosing belt symmetry index

The rate of talweg migration can be used to quantitatively reveal some of the characteristics of channel evolution and is calculated (Giardino and Li, 2011), as follows:

$$R_m = \frac{A}{L} \Big/ y \tag{2}$$

In this expression, R_m denotes the annual talweg migration rate, A is the area surrounded by these lines in two years (i.e., the combined left and the right change area in the latter year relative to the earlier year), while L is length in an earlier year, and y denotes the number of interval years (Figure 4).

Annual talweg migration rates for the six time periods considered in this study are shown in Figure 5; data for the three successive periods between 1990 and 2001, 2001 and 2013, and 2013 and 2016 are shown in Figure 5a, while Figure 5b shows data for the three longer time periods between 2001 and 2016, 1990 and 2013, and 1990 and 2016.

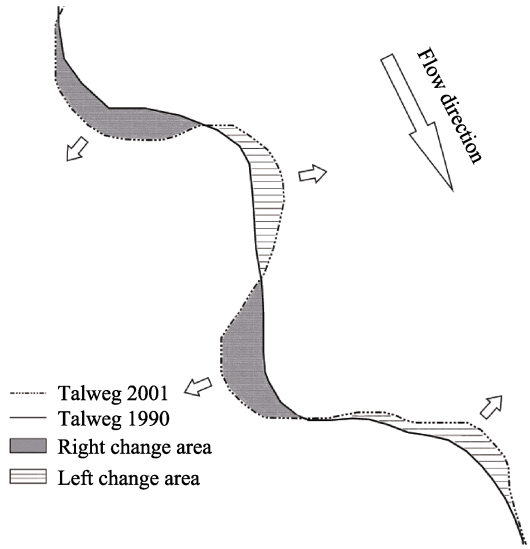

Figure 4 Cartoon showing change in area with talweg migration to either the left or right over time

Data show that the size of the talweg change area on the left and right changed alternately over the three successive periods. The total change area and the annual change rate initially decreased and then increased, with the smallest values, 0.57 km^2 and 3.75 m/yr, recorded between 2001 and 2013, and the largest values, 0.96 km^2 and 25.06 m/yr, recorded between 2013 and 2016, respectively. Results also reveal that some parts of the talweg underwent discontinuous change between 2013 and 2016 (Figure 2) which led to a much larger change area and rate.

In contrast, the area of total change was larger over the three longer time periods than that in the three successive periods, and annual rates of change were 6.45 m/yr, 3.37 m/yr, and 4.63 m/yr, respectively. Recorded rates of change were relatively smaller over longer time periods; the talweg rate of change was 3.37 m/yr between 1990 and 2013, the smallest of all periods, but was larger between 1990 and 2016 than between 1990 and 2013 because of the discontinuous change to this line that occurred between 2013 and 2016.

The watershed symmetry index (R_s), the ratio between the right and left side areas of the talweg within a basin, was proposed by Qian *et al*. (1987) as a proxy for watershed symmetry. Building on this, we propose use of the anastomosing belt symmetry index (SI_a) in this study, the ratio between right and left side areas divided by the talweg within an anastomos-

ing belt. The index comprises a dimensionless number and can be used to reflect either the symmetry of an anastomosing belt or trends in the relative migration of the talweg. Thus, when SI_a increases, the talweg migrates to the left, while when SI_a decreases, the talweg migrates to the right.

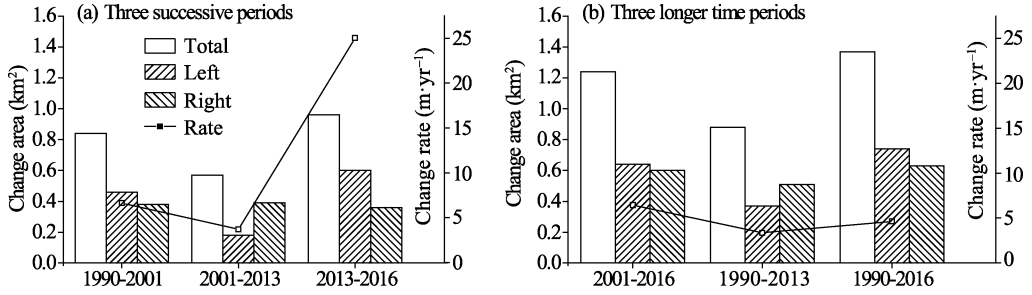

Figure 5 Changes in area caused by talweg migration within different time periods and the mean annual rate of change within the river reach studied in this paper

The data presented in Figure 6 show that right side area remained consistently greater than left side area divided by the talweg within the river anastomosing belt. Thus, measured values of SI_a ranged between 1.59 and 1.70 over the course of this study; SI_a increased from 1.69 to 1.70 between 1990 and 2001 which means that the talweg migrated to the left, while because this index decreased from 1.70 to 1.59 between 2001 and 2013, the talweg migrated to the right. In contrast, SI_a values increased from 1.59 to 1.65 between 2013 and 2016, indicating that this line migrated to the left. These data accord with the observation that the area of left talweg change was greater, smaller, and greater than that seen on the right over the three successive time periods of this study (Figure 5).

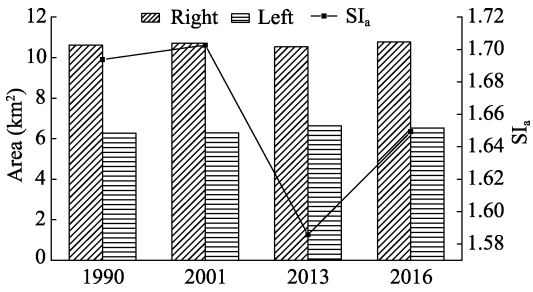

Figure 6 Comparison of symmetry index values for the anastomosing belt in different years

3.3 The influence of talweg migration on interchannel wetlands and river banks

The data presented in Figure 7a show that the talweg migrated to the right between 1990 and 2016, up to a maximum distance of about 270 m. Although the boundaries of the anastomosing belt did not change significantly, associated interchannel wetlands and islands did vary a great deal; as the talweg migrated to the right between 1990 and 2001, island D1 was eroded upstream and deposited downstream, amalgamating with the S1 interchannel wetland. At the same time, the upstream side of island D2 was also eroded but because this corresponded with no obvious downstream side deposition, the whole area was reduced by almost a half. As island D1 was strongly influenced by water flow because of its elevated situation on the talweg curve, sediments in this case were easily blocked by southeastern wetland S1 before being re-deposited.

Observations show that the talweg continuously migrated to the right between 2001 and

2013 causing erosion on the northern side of interchannel wetland S1 and the continuous retreat of the northwestern side of island D1. Erosion also occurred on the upstream side of island D2 over the time period of this study and deposition took place downstream side, with the area of the latter much larger than the former. Similarly, although the upstream side of island D2 only experienced a small amount of erosion between 2001 and 2013, its downstream side was extended about 200 m to the southwest because of sedimentation while the southeastern side of wetland S2 also experienced deposition.

The field data incorporated in this study (Table 2) show that the interchannel wetland to the right of sampling site QP26 is 2 m high and incorporates an uppermost 1 m mud layer and a basal 1 m gravel layer. Field observations show that about 1 m of the southeastern part of the interchannel wetland S2 has been deposited over the last decade, and that because a new island (D3) is developing between wetlands D2 and S2, the channel between the two must have been deposited between 2001 and 2013. Observations also show that the right side of the main channel was relatively higher in the past, and that a gravel bar extended upstream to the north of QP27 (Table 2). A large number of fallen trees within interchannel wetland S2 were also recorded to the west of QP28; this is consistent with the presence of a branching node that diverted more water flow to the right as the talweg migrated in this direction which led to erosion of the right bank of the main channel. The topography downstream of QP28 was also higher in the past which means that less sediments have been transported in this direction than have been deposited due to a backwater effect. At the same time, the water flow is weaker on the downstream side of island D3 because of this backwater effect, which has also led to deposition on both side of QP26; thus, three new islands (D4, D5, and D6) appeared on the left side of the talweg causing its migration to the right and deposition on the side of these new features.

In addition, although the talweg significantly migrated to the right between 2013 and

Table 2 The locations of field work sites and the characteristics of columnar sections on the channel banks of the Qihama reach of the anastomosing river in 2016

Site	Observation date	Latitude	Longitude	Channel and sediment characteristics
QP25	April 26th	33°22′51″N	102°01′20″E	The upper layer of the left main channel bank at this site is composed mainly of fine sand and silt, while the lower layer below 75 cm is gravel.
QP26	April 30th	33°22′33″N	102°00′36″E	The width of the right anastomosing channel is 60 m, the water width is 30 m, and the water depth is 1 m at this location. The bank height is 2 m, with 1 m mud layer on the top and 1m gravel layer on the bottom. The mean size of gravel is between 6 cm and 7 cm, ranging up to a maximum of 10 cm.
QP27	April 30th	33°22′43″N	102°00′40″E	The main channel width at this site is about 200 m and comprises two gravel bars in the center and one gravel bar adjacent to the right bank which had been eroded about 1 m.
QP28	April 30th	33°22′46″N	102°00′36″E	The width of the anastomosing channel adjacent to the main channel at this site is 15 m and an upward extending gravel bar with a maximum width of 30 m is next to the left bank of the main channel. The right bank at this site is about 1.6 m high and has a 1 m mud layer on the top and a 0.6 m gravel layer on its base. A large number of trees on the right bank were fallen, indicating that this right bank was washed back.

2016, no significant changes were seen in the adjacent interchannel wetlands. This means that it is difficult to erode the channel bank over the short-term process of talweg migration.

The area where the anastomosing belt changed most obviously is shown in Figure 7b. These data show that the right side of the main channel encompasses the S1 interchannel wetlands, while the left side comprises the margin of the anastomosing belt or the bank of the main channel on this side. No anastomosing channel developed on the left concave bank of the main channel while it was subject to strong erosion while its boundary also did not significantly change. Observations show that the maximum migration distance of this bank between 1990 and 2016 was about 130 m, while the annual rate of change was 5 m/yr; similarly, the width of the anastomosing belt within this region was about 2000 m, corresponding with an approximately 0.25% annual rate of change. Although the main bank of this channel has been strongly affected by water flow, its retrogradation rate has nevertheless been very slow, indicating that the margin directly affected by talweg migration is also very stable.

3.4 The evolutionary characteristics of anastomosing channels

Because of the issues inherent to studying the evolution of a single small anastomosing channel using Landsat images that have resolutions of either 15 m or 30 m, two high resolution GE images (0.5 m resolution) for 2011 and 2013 were also utilized in this study to vectorize and analyze the four anastomosing channels (lower right corner of Figure 7).

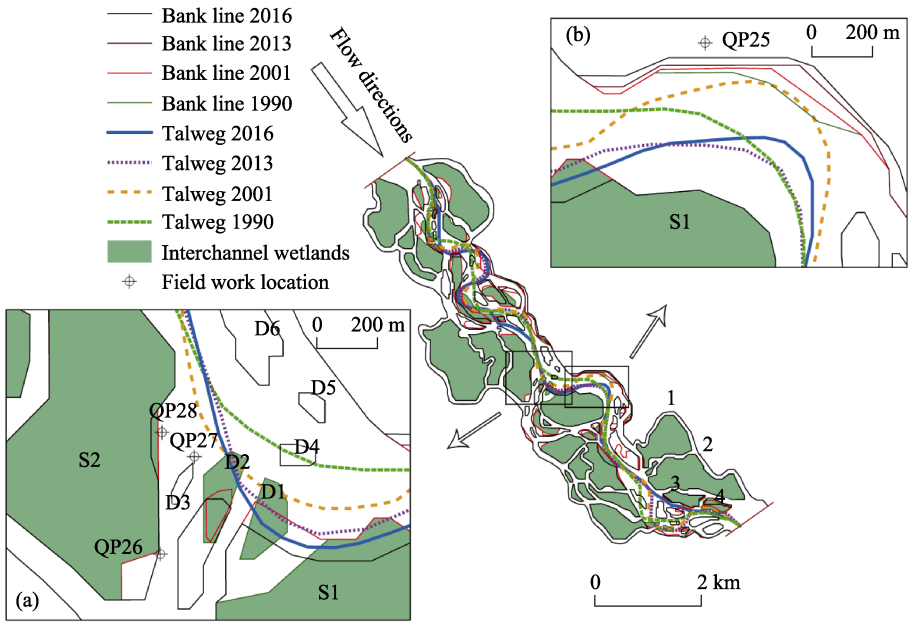

Figure 7 Changes in the talweg, interchannel wetlands, and banks within typical sections of the study river reach

Changes in the area, length, sinuosity, and mean width of the four anastomosing channels within the river reach studied in this paper between 2011 and 2013 are shown in Figure 8. Data show that the areas of channels 1, 2, and 3 slightly decreased over this time period by 6.57%, 6.06% and 6.38%, respectively, while the area of channel 4 increased by 1.24% (Figure 8a). Similarly, the lengths of channels 1 and 2 also increased slightly (by 1.47% and 1.20%, respectively) while the lengths of channels 3 and 4 decreased slightly (by 0.60% and

0.64%, respectively) (Figure 8b). At the same time, the mean widths of channels 1, 2, and 3 also decreased slightly (by 7.92%, 7.18%, and 5.82%, respectively), while the mean width of channel 4 increased by 1.89% (Figure 8c). The corresponding lateral accretion rates of these four channels were 1 m/yr, 1.5 m/yr, 1 m/yr, and –0.5 m/yr, respectively, while variations in their sinuosity were very small, all rates less than 2.73% (Figure 8d).

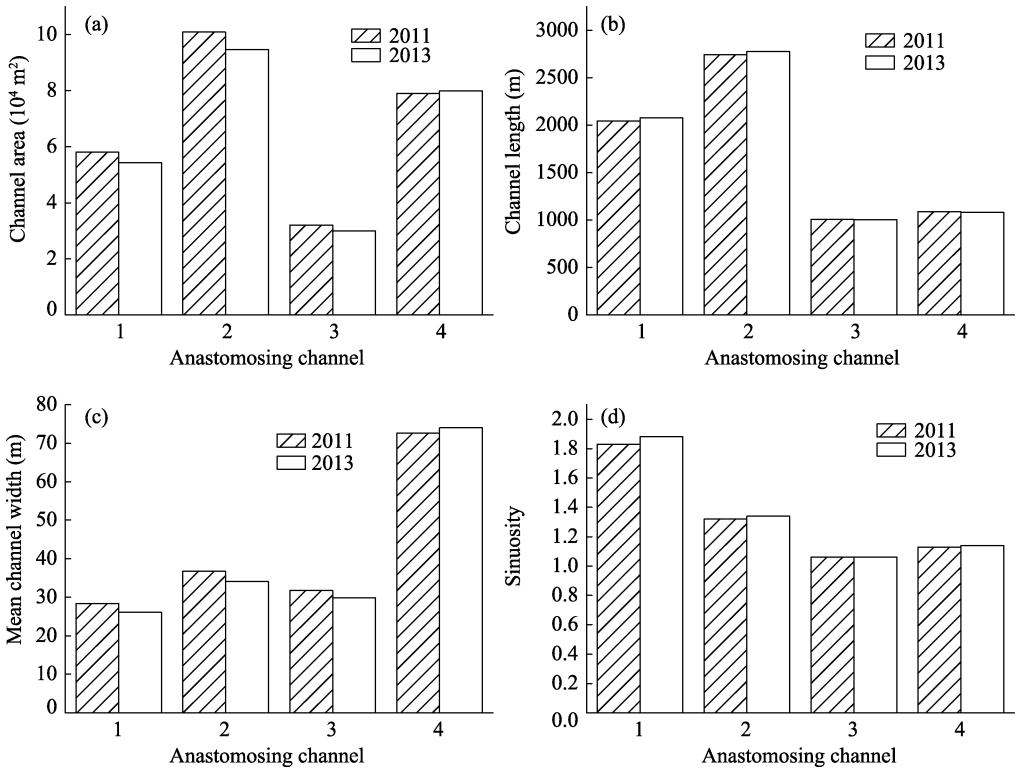

Figure 8 Comparison of the four anastomosing channel planforms within the river reach of the study area between 2011 and 2013

4 Discussion

The avulsion model for the formation of anastomosing rivers was summarized in three successive stages by Smith (1989) and Wang (2002) as comprising initial multi- and anastomosing-channelization followed by the development of a regular anastomosing channel. Observations show that the river reach studied here developed during the third of these stages because the entire anastomosing belt is adequately developed, the locations of channels are basically stable, and the ratio between water and land area maintained relatively constant throughout the study period. The total area of the anastomosing belt also increased slightly while interchannel wetlands became fragmented.

The results of this study show that while the talweg migrated alternately to the left and right over time, its rate of change remained relatively stable over a longer period and exerted little influence on the entirety of the anastomosing belt. Indeed, because of the stability of the anastomosing belt, recorded SI_a values generally ranged between 1.60 and 1.70; this variation reflects the fact that actual trends in talweg migration are consistent with relative trends. The recorded migration rate of the main channel is also visibly larger than that of the

anastomosing ones based on talweg data, a characteristic that is more reminiscent of meandering than anastomosing rivers. Previous studies (e.g., Smith *et al*., 1989; Mccarthy, 1992; Wang *et al*., 2004, 2005) have noted that anastomosing rivers form via early channel avulsion; indeed, rivers of this type within the Jingjiang reach of the Yangtze River and within the middle reaches of the Amazon River all developed via an avulsed channel splitting from the meandering river (Wang, 2002; Soares *et al*., 2010; Rozo *et al*., 2012). The research presented here on the anastomosing river within the Jingjiang reach of the Yangtze River demonstrates that some anastomosing channels can be very stable and that lateral migrations are not obvious; this contrasts with the main Yangtze River channel that is very unstable and exhibits a lateral migration rate greater than about 30 m/yr (Wang *et al*., 2005). The mean annual migration rate of the left bank of the meandering-similar main channel reported in this study was less than 5 m/yr, much smaller than that of the Jingjiang meandering channel. At the same time, however, the migration rate of anastomosing channels within the Qihama river reach reported here is almost equal to that seen in the Yangtze where the rate is 1 m/yr (Wang *et al*., 2005). This suggests that the anastomosing channels within the Qihama river reach are at least as stable as their counterparts within the Yangtze.

The typical sediment characteristics of this river section are epitomized by data from sampling point QP25 on the left bank and sampling point QP27 on the right bar of the main channel (Figure 7). Samples were taken at these points from the surface and at depths every 15 cm at QP25 and every10 cm at QP27 and show that sediments from below a depth of 75 cm in QP25 and 120 cm in QP27 are gravel layers (Figure 9). Thus, comparing the data presented in Figures 9a and 9b, it is clear that the sediments that comprise the bar and the bank of this channel are mainly composed of fine sand and silt, while the clay content is high and there is a multi-peak grain-size distribution curve. The mean clay content at these two sampling sites is about 10%, although the value (14.90%) at QP27 is higher than that at QP25 (8.01%) and there is also a clear difference in sand content. Similarly, the mean fine sand content (50.64%) is higher than the silt content (34.68%) in sample QP25, while the mean silt content (53.97%) is higher than the fine sand content (29.67%) in sample QP27, and mean coarse sand content (10.92%) is higher in QP25 but much smaller (1.40%) in QP27. These data show that the sediment characteristics of the channel bank and the bar are similar, but the materials within the latter are finer because of the deposition of suspended sediment.

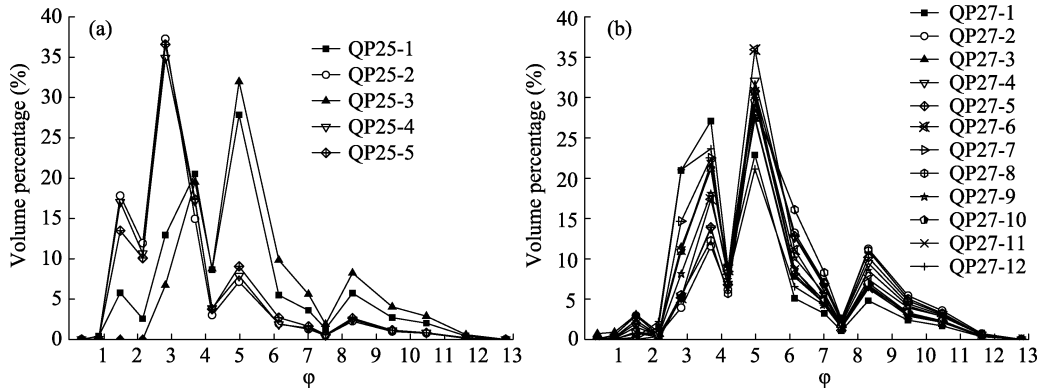

Figure 9 Percentage distribution curves for different grain sizes within the bank columnar sections QP25 (a) and QP27 (b)

The data presented in this paper show that while the riverbed within anastomosing channels consists of gravel, sediments on top are mainly silt and mud, a minor difference from the clay that makes up sand-bedded anastomosing channels, including those within the Yangtze River. The presence of dense vegetation within riparian and interchannel wetlands protects these anastomosing channel banks from erosion, and maintains their stability. Thus, the high lateral migration rate that characterizes the main channel is the result of strong stream power and the relatively lower cohesiveness of bank sediments. It is also the case, however, that many of these anastomosing channels remain in active for some months of the year or even operate at a low flow rate; combined with a narrow channel and vegetation-covered midchannel wetlands, this results in high stability and limited lateral migration. Although the crust within the study area is the result of tectonic uplift, anastomosing reach is nevertheless in subsidence relative to the surrounding high ground, and generally illustrates that the main channel is slightly eroded surrounding anastomosing channels and interchannel wetlands are more obviously the result of deposited. It is noteworthy that Makaske *et al*. (2009) noted in earlier work that the anastomosing section in the upper reaches of the Columbia River formed via avulsion due to river bed sedimentation. The gravel-bedded anastomosing river studied in this paper also exhibits a number of similarities to sandy-bedded rivers of this type in terms of channel planforms and stability. However, an increase in the number of interchannel wetlands with time indicates that some small new channels formed within individual midchannel wetlands via the avulsion of old channels; this observation, combined with hydrodynamic conditions and sedimentary characteristics, highlight clear differences from sandy-bedded anastomosing rivers. Further research will therefore be required to determine the specific processes that led to the formation of this river channel.

5 Conclusions

A number of clear conclusions regarding the characteristics and evolution of the gravel-bedded anastomosing river within the Qihama reach of the First Great Bend of the Yellow River over the last 26 years can be presented based on the channel planform and sediment composition analyses presented in this paper.

(1) Gravel-bedded anastomosing channels tend to exhibit a high degree of stability. Data show that over the last 26 years, the area of the anastomosing belt of this river channel has increased from 16.89 km^2 to 17.30 km^2, an annual rate of increase of 2.43%, while the ratio of land to water area has remained almost equal. At the same time, the number of interchannel wetlands that comprise small areas between 0.1 km^2 and 0.8 km^2 has markedly increased, at a rate as high as 62.16%. Although this anastomosing belt fragmented over time, changes in the areas of larger interchannel wetlands were not obvious.

(2) The main channel talweg migrated alternately to the left or right over the time period of this study, at a rate that remained relatively stable. Data show, however, that the trend in talweg migration remained consistent with the actual trend at least on the basis of SI_a changes. Indeed, because of the influence of talweg migration, large changes to the islands within the main channel have been seen while the maximum annual change rate of the outer bank has remained around 5 m/yr, similar to the characteristics of a meandering river. The numerous anastomosing channels have remained very stable with a mean annual migration rate about 1 m/yr.

(3) The surface sediments that comprise midchannel bars and river banks are mainly fine sands and silts. These sediments have a relatively high clay content (about 10%) and exhibit a multi-peak grain-size distribution curve. At the same time, gravel makes up the beds of anastomosing channels, a significant difference from sand-bedded rivers of this type. Bank sediments, however, are mainly silt and clay, another slight difference from the clay banks of sand-bedded anastomosing rivers, while the presence of dense vegetation on riparian and interchannel wetlands protects these anastomosing channels from erosion and maintains their stability. These sediments are also an important factor contributing to the high stability of this gravel-bedded anastomosing river system.

References

Giardino J R, Lee A A, 2011. Rates of channel migration on the Brazos River [D]. Yangling: Department of Geology & Geophysics, Texas A & M University.

Gurnell A M, 2015. Channel change on the River Dee meanders, 1946–1992, from the analysis of air photographs. *River Research & Applications*, 13(1): 13–26.

Knighton A D, Nanson G C, 1993. Anastomosis and the continuum of channel pattern. *Earth Surface Processes and Landforms*, 18(7): 613–625.

Li J, Fang X, Ma H *et al*., 1996. Landform evolution of the upper reaches of the Huanghe River in late Cenozoic era and the upwelling of the Qinghai-Tibet Plateau. *Science in China* (*Series D*), 26(4): 316–322. (in Chinese)

Li Z, Wang Z, Yu Guoan *et al*., 2013. River pattern transition and its causes along the Maqu reach of the Yellow River source region. *Journal of Sediment Research*, (3): 51–58. (in Chinese)

Liu B, Wang S, 2017. Planform characteristics and developing of interchannel wetlands in a gravel-bed anastomosing river, Maqu reach of the Upper Yellow River. *Journal of Geographical Sciences*, 27(11): 1376–1388.

Makaske B, 2001. Anastomosing rivers: A review of their classification, origin and sedimentary products. *Earth Science Reviews*, 53(3/4): 149–196.

Makaske B, Smith D G, Berendsen H J A *et al*., 2009. Hydraulic and sedimentary processes causing anastomosing morphology of the upper Columbia River, British Columbia, Canada. *Geomorphology*, 111(3/4): 194–205.

Mccarthy T S, Ellery W N, Stanistreet I G, 1992. Avulsion mechanisms on the Okavango fan, Botswana: The control of a fluvial system by vegetation. *Sedimentology*, 39(5): 779–795.

Murray A B, Paola C, 1994. A cellular model of braided rivers. *Nature*, 371(6492): 54–57.

Murray A B, Paola C, 2015. Properties of a cellular braided-stream model. *Earth Surface Processes and Landforms*, 22(11): 1001–1025.

Qian N, Zhang R, Zhou Z, 1987. Fluvial Process. Beijing: Science Press. (in Chinese)

Rozo M G, Nogueira A C R, Truckenbrodt W, 2012. The anastomosing pattern and the extensively distributed scroll bars in the middle Amazon River. *Earth Surface Processes and Landforms*, 37(14): 1471–1488.

Rust B R, 1978. A classification of alluvial channel systems. In: Miall A D. Fluvial Sedimentology. Canada Calgary: Canadian Society of Petroleum Geologists, 187–198.

Rust B R, 1981. Sedimentation in an arid-zone anastomosing fluvial system: Cooper's Creek, central Australia. *Journal of Sedimentary Research*, 51(3): 745–755.

Schumm S A, 1985. Patterns of alluvial rivers. *Earth and Planetary Sciences*, 13(13): 5–27.

Schumm S A, 1968. River adjustment to altered hydrologic regimen, Murrumbidgee River and paleochannels, Australia. *Center for Integrated Data Analytics Wisconsin Science Center*, 43(177): 110–110.

Selby M J, 1985. Earth's Changing Surface. An introduction to geomorphology. *Economic Journal*, 112(476): 93–106.

Shi C, Wu B, Ma J, 2007a. Cause of formation and discrimination of channel patterns for alluvial rivers. *Journal of Hydroelectric Engineering*, 26(5): 107–111. (in Chinese)

Shi C, Wu B, Ma J, 2007b. Classification and discrimination of channel patterns in the Lower Yellow River. *Journal of Sediment Research*, (4): 53–58. (in Chinese)

Shi C, Wu B, Ma J, 2009. Natural classification of river patterns based on clustering method with fuzzy equiva-

lent matrices. *Journal of Hydroelectric Engineering*, 28(5): 215–220. (in Chinese)

Smith D G, 1983. Anastomosed fluvial deposits: Modern examples from western Canada. *Modern and Ancient Fluvial Systems*, 155–168.

Smith D G, Putnam P E, 1980. Anastomosed river deposits: Modern and ancient examples in Alberta, Canada. *Canadian Journal of Earth Sciences*, 17(10): 1396–1406.

Smith D G, Smith N D, 1980. Sedimentation in anastomosed river systems: Examples from alluvial valleys near Banff, Alberta. *Journal of Sedimentary Research*, 50(1): 157–164.

Smith N D, Cross T A, Dufficy J P *et al*., 1989. Anatomy of an avulsion. *Sedimentology*, 36(1): 1–23.

Soares E A A, Tatumi S H, Riccomini C, 2010. OSL age determinations of Pleistocene fluvial deposits in central Amazonia. *Anais Da Academia Brasileira De Ciências*, 82(82): 691–699.

Thomas R, Nicholas A P, 2002. Simulation of braided river flow using a new cellular routing scheme. *Geomorphology*, 43(3–4): 179–195.

Tornqvist T E, 1993. Holocene alternation of meandering and anastomosing fluvial systems in the Rhine-Meuse delta (central Netherlands) controlled by sea-level rise and subsoil erodibility. *Journal of Sedimentary Research*, 63(4): 683–693.

Udden J A, 1914. Mechanical composition of clastic sediments. *Geological Society of America Bulletin*, 25(1): 655–744.

Wang P, 1990. A fuzzy mathematical method on the classification of river patterns. *Journal of Chengdu University of Science and Technology*, (1): 83–93. (in Chinese)

Wang S, 2002. Comparison of formation model and channel stability between two different sorts of multiple channel river patterns. *Acta Geoscientia Sinica*, 23(1): 89–93. (in Chinese)

Wang S, 2008. Analysis of river pattern transformations in the Yellow River basin. *Progress in Geography*, 27(2): 10–17. (in Chinese)

Wang S, Chen Z, Smith D G, 2005. Anastomosing river system along the subsiding middle Yangtze River basin, southern China. *Catena*, 60(2): 147–163.

Wang S, Li J, Yin S, 1999. Basic characteristics and controlling factors of anastomosing fluvial systems. *Scientia Geographica Sinica*, 19(5): 422–427. (in Chinese)

Wang S, Li L, Cheng W, 2014. Variations of bank shift rates along the Yinchuan Plain Reach of the Yellow River and their influence factors. *Journal of Geographical Sciences*, 24(4): 703–716.

Wang S, Mei Y, 2016. Lateral erosion/accretion area and shrinkage rate of the Linhe reach braided channel of the Yellow River between 1977 and 2014. *Journal of Geographical Sciences*, 26(11): 1579–1592.

Wang S, Ni J, Wang G *et al*., 2004. Hydrological processes of an anastomosing river system on the Zhujiang River Delta, China. *Journal of Coastal Research*, 124–133.

Wang S, Ren M, 1999. A new classification of fluvial rivers according to channel planform and sediment characteristics. *Acta Sedimentologica Sinica*, 17(2): 240–246. (in Chinese)

Wang S, Xie X, Cheng D, 2002. The progress in the research of anastomosing river. *Progress in Geography*, 21(5): 440–449. (in Chinese)

Wang S, Yin S, 2000. Discussion on channel patterns of anastomosing and anabranched rivers. *Earth Science Frontiers*, (s2): 79–86. (in Chinese)

Wentworth C K, 1922. A scale of grade and class terms for clastic sediments. *The Journal of Geology*, 30(5): 377–392.

Xu X, Shi C, 2009. Analysis on basis and mathematical method of channel classification of alluvial river. *Journal of Yellow River Conservancy Technical Institute*, 21(1): 7–9. (in Chinese)

Yan M, Wang S, Yan Y *et al*., 2013. Planar changes of upper alluvial reaches of the Yellow River in recent thirty years. *Journal of Arid Land Resources and Environment*, 27(3): 74–79. (in Chinese)

Yang D, Wang Y, 1996. On river terraces of the upper reaches of the Huanghe River and change of the river system. *Scientia Geographica Sinica*, 16(2): 137–143. (in Chinese)

Yuan B, Wang Z, 1995. Uplift of the Qinghai-Xizang Plateau and the Yellow River physiographic period. *Quaternary Sciences*, (4): 353–359. (in Chinese)

Zhang Z, Yu Q, Zhang K *et al*., 2003. Geomorphological evolution of a Quaternary river from the upper Yellow River and geomorphological evolution investigation for 1:250000 scale geological mapping in Qinghai-Tibet Plateau. *Earth Science-Journal of China University of Geosciences*, 28(6): 621–626. (in Chinese)